Biosensors and Bioelectronics 91 (2017) 706–713

Contents lists available at ScienceDirect

Biosensors and Bioelectronics

journal homepage: www.elsevier.com/locate/bios

Gold nanrods plasmon-enhanced photoelectrochemical aptasensing based on hematite/N-doped graphene films for ultrasensitive analysis of 17β-estradiol

Xiaojiao Du[a,1], Liming Dai[a,1], Ding Jiang[b], Henan Li[a], Nan Hao[a], Tianyan You[a], Hanping Mao[a], Kun Wang[a,*]

[a] Key Laboratory of Modern Agriculture Equipment and Technology, School of Chemistry and Chemical Engineering, Jiangsu University, Zhenjiang 212013, PR China

[b] School of Food and Biological Engineering, Jiangsu University, Zhenjiang 212013, PR China

ARTICLE INFO

Keywords:
Surface plasmon resonance
Au nanorod
Photoelectrochemical aptasensor
17β-estradiol

ABSTRACT

It remains a vital task to establish ultrasensitive sensing interfaces for detection of target analytes to meet the demands of modern analysis. Herein, a highly sensitive turn-on photoelectrochemical (PEC) platform for trace 17β-estradiol (E2) assay was developed based on Au nanrods (AuNRs) with surface plasmon resonance (SPR) properties induced signal amplification. Specifically, a ternary hybrid was prepared by integrating hematite (α-Fe_2O_3) nanocrystals and N-doped graphene (NG) with AuNRs, which further served as highly efficient photoactive species. Subsequently, a PEC sensing platform was fabricated based on the specific binding of E2 and its aptamer. On such a sensor, the capture of E2 molecules by aptamers led to increased photocurrent. This was attributed to that the specific recognition reaction between E2 and aptamer resulted in the conformational change of the aptamers and complete dissociation of some aptamers on the PEC sensing interface. It can be confirmed by the electrochemical impedance spectroscopy (EIS) results. This process decreased the steric hindrances between the electrode surface and solution and thus increased the photocurrent response. Under the optimal conditions, the as-prepared PEC aptasensor exhibited superb analytical performances for detection of E2 in the range from 1×10^{-15} M to 1×10^{-9} M with a detection limit of 3.3×10^{-16} M. The aptasensor manifested outstanding selectivity towards E2 when other endocrine disrupting compounds with similar structure coexisted. Furthermore, the aptasensor was successfully applied for the determination of E2 in milk powder. The present strategy provides a potential way to boost the activity of photoactive materials and improve the sensitivity of PEC biosensor.

1. Introduction

17β-estradiol (E2), as a natural estrogen and a typical endocrine disrupting chemical, has been widely used in the livestock and poultry industry (Pezzolato et al., 2011), to promote animal growth, improve lean meat proportion, and increase milk yield (Han et al., 2016). However, E2 residues can also lead to premature puberty, increase exposure to the risk of ovarian and breast cancer. Most noteworthy is that humans would be affected notably as a result of bio-concentration through food chain even at E2 concentration level as low as pg~ng/L, as it can cause the severe health problems, such as growth abnormality, infertility, the decline of the male reproductive function, and the increasing incidence of cancers (Ke et al., 2014). Therefore, a large number of classical E2 detection techniques, such as gas chromatography (Shrestha et al., 2012), high performance liquid chromatography (Tai et al., 2005), gas chromatography-mass spectrometer (Draisci et al., 1998), and liquid chromatography-mass spectrograph (Terne et al., 2002), have been developed. Although these detection techniques are highly sensitive and selective, they require costly equipment, tedious procedures and so forth. Consequently, they are not suitable for fast and low-cost detection of E2 in practical applications. As an alternative method, electrochemical technique is an effective analytical method, possessing the advantages such as low cost, fast response, and environmentally friendly nature. Nevertheless, due to the poor electroactivity of E2, it is difficult to quantify by direct electrochemical oxidation (Song et al., 2008), as it needs high electric potential to

* Corresponding author.
E-mail address: wangkun@ujs.edu.cn (K. Wang).
[1] These authors contributed equally to this work.

http://dx.doi.org/10.1016/j.bios.2017.01.034
Received 7 November 2016; Received in revised form 9 January 2017; Accepted 17 January 2017
Available online 18 January 2017
0956-5663/

oxidize E2, while other substances coexisting in the detecting system can be oxidized simultaneously, thus interfering with the effectiveness of E2 detection in real sample analysis (Ke et al., 2014). To tackle these issues, it is urgently required to develop a route with high performances for the determination of trace E2.

The photoelectrochemical (PEC) sensing is an ultrasensitive method owing to the total separation and different energy form of the excitation (light) and the detection (current), which has been extensively applied to ultrasensitive detection of a wide range of analytes (Fan et al., 2014; Ma et al., 2016). It takes advantages of photocatalytic oxidation with the electrical bias as an auxiliary, generating a sharp photocurrent change in the presence of analytes, avoiding the expensive equipment of optical techniques and high overpotential in electrochemistry measurements (Zhang et al., 2013). Thereinto, a critical issue is how to further improve its sensitivity and get ameliorative analytical performance, and meanwhile the first premise of sensitivity improvement is to obtain enhanced photocurrent (Zhang et al., 2016). Up to now, many approaches have been developed for PEC sensing to enhance the photocurrent, including dye sensitization (Zhang et al., 2010), graphene-semiconductor composites (Zhao et al., 2012b; Tu et al., 2012), semiconductor heterojunctions (Zhao et al., 2012a), and plasmon-enhanced PEC sensing (Zhang et al., 2016; Li et al., 2014a). Among them, PEC sensors based on surface plasmon resonance (SPR), a newly emerging but dynamically developing mean to improve the PEC performance, have been a hot topic recently (Yan et al., 2016). SPR of noble metallic (Au, Ag, Pt) nanostructures is known to concentrate and scatter incident light over a broad wavelength range and holds the promise of enhancing the light absorption cross section of a semiconducting material around the plasmonic structures (Abe et al., 2010; Zhou et al., 2012). As a result, the combination of plasmonic metal with semiconductor has become a flexible routine for enhancing photocurrent response of semiconductor nanostructures. In particular, the SPR of Au can not only act as light harvesting antennae for semiconductors, but also enhance the efficiency of photocurrent transfer, which make it promising in the development of PEC-based sensors with high performances (Abe et al., 2010). Furthermore, as compared to spherical Au nanoparticles, Au nanorods (AuNRs) possess much more interesting optical properties, such as stronger and tunable absorption (the longitudinal plasmon oscillation) (Zhou et al., 2012; Eum et al., 2010). Since unique longitudinal plasmon wavelengths of AuNRs (> 600 nm) are more sensitive to the changes in the dielectric properties of the surroundings, AuNRs are much more sensitive for the quantification of biological molecules than nanoparticles with spherical structure (Zhang et al., 2012). Moreover, in the surface configuration, photoactivity enhancement is observed in the SPR region of AuNRs due to the spectral overlap of absorption of AuNRs and hematite (α-Fe_2O_3) catalyst (Thimsen et al., 2011). As a result, it is feasible to improve the PEC activity for analyte-sensing applications by coupling AuNRs with α-Fe_2O_3 absorption based on SPR effect (Warren and Thimsen, 2012; Kochuveedu et al., 2011).

In the process, this PEC technique encounters the problem of selectivity. As a consequence, how to realize the selective recognition of E2 in a PEC sensing system remains a substantial challenge. Aptamer-based methods have been considered as certainly highly promising candidates for the specific detection of their targets in recent years (Ho et al., 2004). Aptamers, a kind of high affinity and specific molecular recognition elements, have been successfully synthetically evolved to recognize target molecules such as amino acids, protein and small molecules (Ellington et al., 1990; Tuerk et al., 1990; McKeague et al., 2012). They posses much more advantages over the traditional recongnition elements due to their non toxicity, specific binding ability, and good stability during long-term storage (Neumann et al., 2009). In the case of low molecular weight targets E2, the binding is associated with conformational switching of the aptamer (Citartan et al., 2012). Binding signals can then be transduced via colorimetric (Alsager et al., 2015), fluorescence (Sassolas et al., 2011), and electrochemical responses (Li et al., 2015b; Fan et al., 2014). Thus, the combination of PEC and aptamer technique will be viable to build an excellent sensing platform for E2 detection with high sensitivity and selectivity.

In this work, AuNRs were designed to modify the α-Fe_2O_3 nanocrystals anchored on the N-doped graphene (NG) substances to form ternary α-Fe_2O_3-NG-AuNRs hybrids, which further acted as a photoactive substrate for immobilizing the E2 aptamer. The α-Fe_2O_3-NG composites are a kind of perfect PEC sensing material with excellent PEC activity in the visible region due to the synergistic effect between the NG sheets and α-Fe_2O_3 nanocrystals in our recent work (Dai et al., 2017). Moreover, NG with high surface area provides much more space for increasing the load of aptamer molecules and could improve the sensitivity of the aptasensor (Du et al., 2016). Most importantly, by introducing AuNRs, the absorption of α-Fe_2O_3-NG-AuNRs was successfully strengthened in the visible region so that the absorption ability and PEC activity was prompted dramatically. On such a sensor, the capture of E2 molecules by aptamers induces the conformational conversion of aptamer and the recovery of the photocurrent. Therefore, E2 could be quantified via measuring the photocurrent change. Besides, the PEC aptasensor exhibits superior performances in detection of E2 in milk powder, demonstrating the applicability in real samples.

2. Experimental

2.1. Reagents

The 76mer DNA aptamer for E2 was synthesized by Sangon Biotech (Shanghai, China) with sequence as follows (Fan et al., 2014):

5′-GCT-TCC-AGC-TTA-TTG-AAT-TAC-ACG-CAG-AGG-GTA-GCG-GCT-CTG-CGC-ATT-CAA-TTG-CTG-CGC-GCT-GAA-GCG-CGG-AAG-C-3′.

E2 was purchased from Aladdin Chemistry Co., Ltd. Hydrogen tetrachloroaurate (III) ($HAuCl_4$) and $AgNO_3$ were from Sigma-Aldrich (St. Louis, MO) and Shanghai institute of fine chemical material, respectively. Cetyltrimethyl ammonium bromide (CTAB), $NaBH_4$, ascorbic acid (AA), and other routine chemicals were acquired from Sinopharm Chemical Reagent Co., Ltd. α-Fe_2O_3-NG material was prepared according to our recently reported method (Dai et al., 2017). (See Suplementary material).

2.2. Apparatus

The morphologies of the samples were determined using a H800 transmission electron microscope (TEM, Hitachi, Japan). Crystal structure identification was determined using X-ray diffraction (XRD) with a D8 ADVANCE diffractometer (Bruker, Germany) with Cu Kα (λ=1.5406 Å) radiation. Element distribution mappings were obtained from an energy dispersive spectrum (EDS) spectrometer (Hitachi S-4800II, Japan). X-ray photoelectron spectroscopy (XPS, PHI 5000 Versa Probe, Japan) analysis was performed on a Thermo VG Scientific ESCALAB 250 spectrometer using the Mg Kα radiation. Ultraviolet-visible (UV–vis) absorption spectra were measured using a UV-2450 spectrophotometer (Shimadzu, Japan). All the electrochemical and PEC measurements were performed with a CHI 660B electrochemical workstation (Chenhua Instruments Co., Shanghai, China) and recorded by a conventional three-electrode system where an indium tin oxide (ITO) as a working electrode, a saturated calomel electrode (SCE) as a reference electrode, and a platinum (Pt) wire as a counter electrode. PEC measurement was carried out in 0.1 M phosphate buffer solution (PBS) at 0 V and a 500 W Xe lamp (Beijing Chang tuo) was used as the visible light source with 400-nm cut-off filter placed into the path of the Xe lamp to remove the UV irradiation. Electrochemical impedance spectroscopy (EIS) was performed in a 0.1 M KCl solution containing 5 mM $Fe(CN)_6^{3-/4-}$ with a frequency range from 0.01 Hz to 10 kHz at

0.23 V, and the amplitude of the applied sine wave potential in each case was 5 mV.

2.3. Preparation of AuNRs and α-Fe_2O_3-NG-AuNRs

AuNRs were prepared in aqueous solutions using the silver ion-assisted seed-mediated method (Zhou et al., 2012). Explicitly, the seed solution was made by quickly injecting a freshly prepared ice-cold 0.01 M $NaBH_4$ solution (0.6 mL) into an aqueous mixture consisting of 0.1 M CTAB (10 mL) and 1% $HAuCl_4$ (0.103 mL), followed by vigorously stirring for 2 min. Next, the resultant seed solution was kept at 30 °C for 2 h for the subsequent synthesis of AuNRs. Besides, the growth solution was prepared by reduction of 1% $HAuCl_4$ (0.412 mL) in a solution containing 0.1 M CTAB (20 mL) and 0.01 M $AgNO_3$ (0.2 mL). After gentle mixing of the solution, 0.16 mL of AA solution (0.1 M) was added, and the obtained growth solution varied from dark yellow to colorless. Subsequently, the CTAB-stabilized seed solution (0.048 mL) was rapidly added into the growth solution and then the resultant solution was gently mixed for 10 s and left undisturbed 20 h in a 30 °C water bath to initiate the growth process which yielded AuNRs. Afterwards, excess CTAB was removed by centrifuging thrice at 10,000 rpm, the supernatant was discarded, and the particles were redispersed in pure water. The α-Fe_2O_3-NG-AuNRs hybrids were prepared via physical adsorbed method. Typically, AuNRs aqueous solution made by the above method was mixed with α-Fe_2O_3-NG suspension (2 mg/mL) and then underwent ultrasonic treatment to obtain the α-Fe_2O_3-NG-AuNRs hybrids.

3. Results and discussion

3.1. Characterization of the samples

Fig. 1A and Fig. 1B showed the TEM images of the as-prepared AuNRs and α-Fe_2O_3-NG-AuNRs hybrids. According to Fig. 1A, the average size of the AuNRs was about 40 nm. Undergoing this one-pot ultrasonic process, the α-Fe_2O_3 nanocrystal and AuNRs were uniformly anchored onto the surface of NG sheets, which was presented in Fig. 1B. The SPR absorption peak of AuNRs at about 535 nm was characterized by the UV–vis spectrum (Fig. 1C) and the longitudinal peak emission wavelengths of AuNRs at 778 nm (Zhou et al., 2012). Besides, Fig. 1D depicted the typical absorption spectrum of the different materials. The absorption spectrum implied that the α-Fe_2O_3 nanocrystal had a broad absorption range that was suitable for photoactive substrate, even though the absorption intensity of the α-Fe_2O_3 nanocrystal was extremely weak. However, by introducing AuNRs into the α-Fe_2O_3-NG, the absorption intensity of the α-Fe_2O_3-NG-AuNRs hybrids was remarkably enhanced in the visible region, which was attributed to that Au can act as light harvesting antennae that improved the light harvest ability (Yan et al., 2016). Besides, compared with AuNRs, the absorption peak of the α-Fe_2O_3-NG-AuNRs hybrids blue shifted. This is concordant with the previous reports and it might be attributed to the changes of local dielectric environment of AuNRs (Deng et al., 2016; Li et al., 2015a). Moreover, such increased light absorption in the plasmon region in the presence of AuNRs were expected to localize the incident light intensity to help increase the light absorption by the α-Fe_2O_3-NG layer, which are favorable in a PEC system (Archana et al., 2015).

The crystal structure of the prepared samples was characterized by XRD measurement. Fig. S1 displayed the XRD patterns of (a) α-Fe_2O_3-NG and (b) α-Fe_2O_3-NG-AuNRs. The XRD pattern of α-Fe_2O_3-NG-AuNRs depicted diffraction peaks, matching well with the standard peak values of XRD pattern of α-Fe_2O_3 (Joint Committee on Powder Diffraction Standards, JCPDS 33–0664, black color) (Liang et al., 2014). The data for the α-Fe_2O_3-NG-AuNRs exhibited diffraction peaks at 38.18°, 44.39°, 64.58°, and 77.55°, which agreed well with the standard peak values of XRD pattern of Au (JCPDS 04–0784, blue color) (Li et al., 2011; Yu et al., 2015). The XRD results of both α-Fe_2O_3-NG and α-Fe_2O_3-NG-AuNRs also verify that AuNRs have been

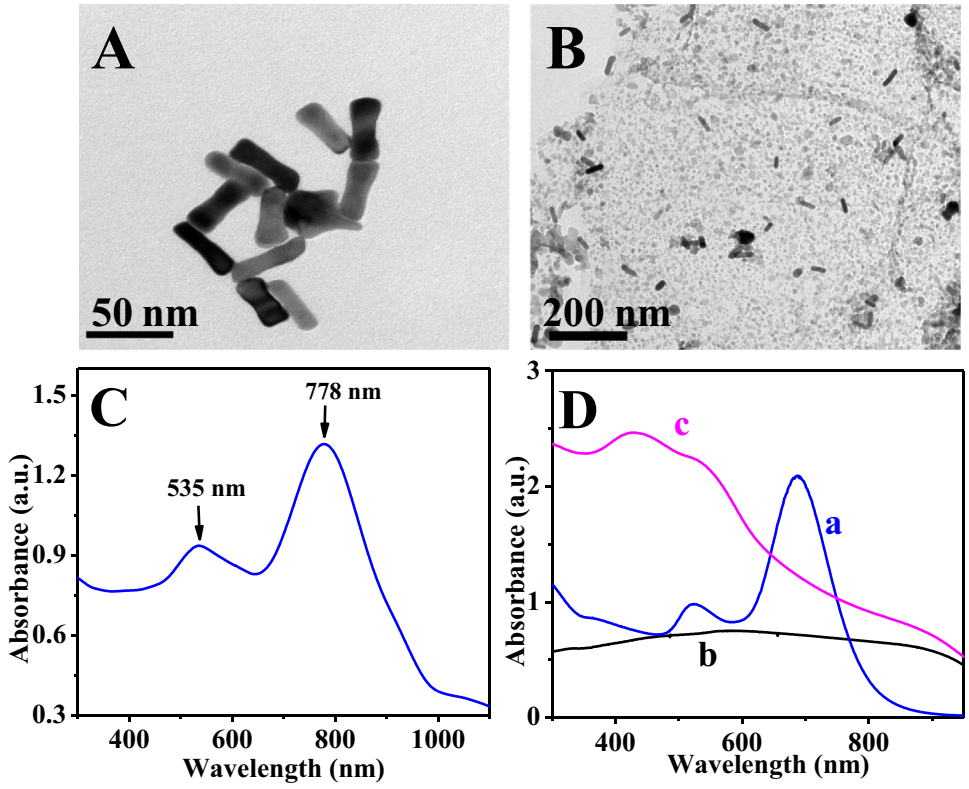

Fig. 1. TEM images of (A) AuNRs and (B) α-Fe_2O_3-NG-AuNRs hybrids; UV–vis spectra of (C) AuNRs and (D) each component of α-Fe_2O_3-NG-AuNRs hybrids (a) AuNRs, (b) α-Fe_2O_3-NG, (c) α-Fe_2O_3-NG-AuNRs.

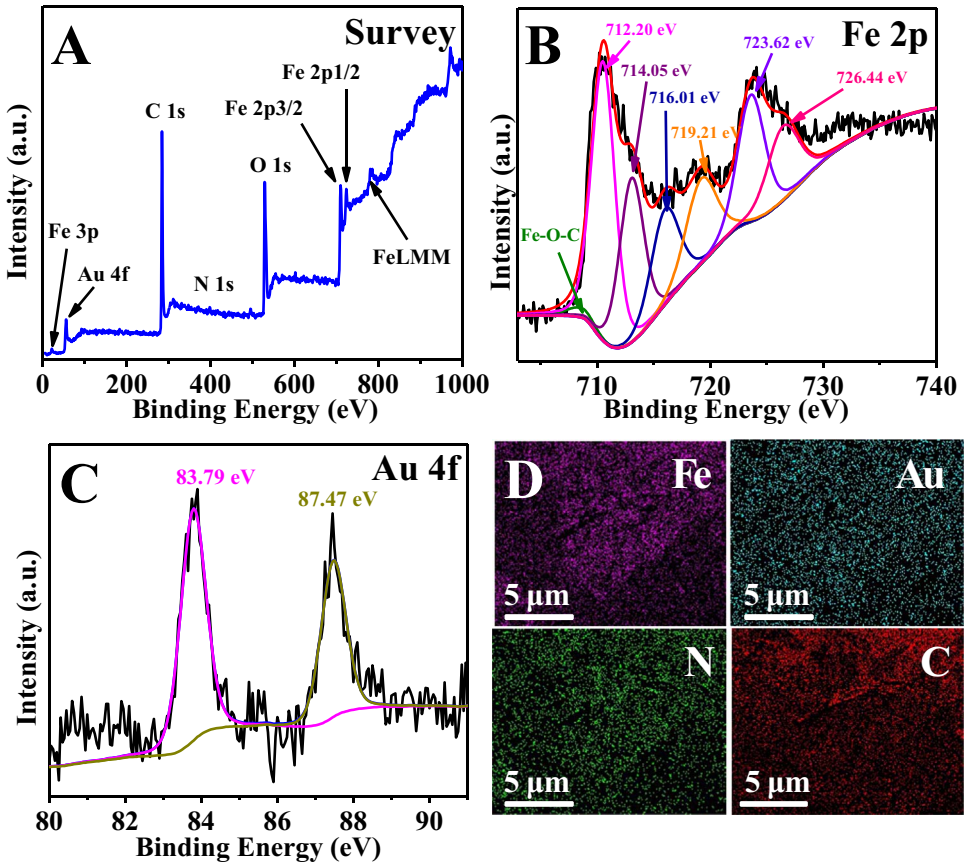

Fig. 2. XPS spectra of the α-Fe_2O_3-NG-AuNRs: (A) survey spectrum and high-resolution spectra of (B) Fe 2p, (C) Au 4f. (D) Element analysis mappings of Fe, Au, N, and C. (For interpretation of the references to color in this figure, the reader is referred to the web version of this article.)

successfully introduced into α-Fe_2O_3-NG.

To further elucidate the structure and chemical composition of the α-Fe_2O_3-NG-AuNRs, XPS measurement was performed, and the results are shown in Fig. 2. The survey spectra exhibited distinctive peaks corresponding to iron (Fe), oxygen (O), carbon (C), nitrogen (N), and gold (Au) elements, confirming the formation of a ternary hybrid (Fig. 2A). The high-resolution XPS spectrum of Fe 2p was deconvoluted into seven multiplet peaks depicted in Fig. 2B. The strongest peaks at 710.24 and 723.55 eV were assigned to the binding energies of the Fe $2p_{3/2}$ and Fe $2p_{1/2}$ levels (Dai et al., 2017). The peak at 712.20 eV represented the hydroxyl groups bonded with Fe^{3+} cations in the ternary hybrid (Yang et al., 2013). The peak at the binding energy of 714.05 eV may be related to α-Fe_2O_3 (Song et al., 2012). Two peaks centered at binding energies of 716.01 and 719.21 eV were associated with the satellite peaks revealed for the hematite nanostructures. Finally, the two additional peaks centered at 723.62 and 726.44 eV indicated the presence of the Fe^{3+} state found in α-Fe_2O_3 (Souza et al., 2009). Besides, it was found that α-Fe_2O_3 nanocrystals, formed strong covalent bond interactions (Fe–O–C bond) with NG, which can be confirmed by analysis of the Fe 2p XPS spectra (Fig. 2B). From the high-resolution spectra of Fe 2p, the peak at 708.9 eV was attributed to the Fe–O–C bond clearly (Zhou et al., 2011; Kataby et al., 1999). The strong covalent links ensured the long-period stability of α-Fe_2O_3-NG nanocomposites. High-resolution Au 4f XPS spectra (Fig. 2C) showed two major characteristic peaks at binding energies of 83.79 and 87.47 eV, corresponding to Au $4f_{5/2}$ and Au $4f_{7/2}$ bands, respectively. This result confirmed the presence of Au in the form of an Au° valence state (Pawar et al., 2015; Mao et al., 2013). All these results were in good agreement with the analysis of XRD and TEM.

To intuitively display the Au distribution, the mappings of various elements analysis were carried out. Fig. 2D exhibited the mappings of different elements. The purple, blue, green, and red were differentiation of Fe, Au, N, and C elements, respectively, suggesting that the AuNRs have been distributed on surface of α-Fe_2O_3-NG successfully.

3.2. Characterization of modified electrodes

Fig. 3A displayed the EIS spectra of α-Fe_2O_3-NG/ITO and α-Fe_2O_3-NG-AuNRs/ITO. From Fig. 3A, it could be obtained that the electron transfer resistance (R_{et}) of α-Fe_2O_3-NG-AuNRs/ITO (curve b) were obviously smaller than α-Fe_2O_3-NG/ITO (curve a), suggesting that AuNRs played an important role in the process of electron transfer. As a result, the ternary hybrid α-Fe_2O_3-NG-AuNRs could improve the electron transfer of photoelectrode interface during E2 detection.

Fig. 3C exhibited the EIS diagrams of different electrodes. As expected, the value of R_{et} obtained at the aptamer/α-Fe_2O_3-NG-AuNRs/ITO was larger than α-Fe_2O_3-NG-AuNRs/ITO, suggesting that the negatively charged phosphate backbone of the oligonucleotides produced an electrostatic repulsion force to the $[Fe(CN)_6]^{3-/4-}$. When E2 was captured by the aptamer/α-Fe_2O_3-NG-AuNRs/ITO, a significant decrement in R_{et} was observed. As the aforementioned figures showed, the results demonstrated that the aptasensor interface has been fabricated successfully.

3.3. Characterization of PEC activity

To evaluate the improved activity of photoanodes, systematic PEC measurements were carried out by amperometric *I-t* curves (Formal et al., 2012). Fig. 3B showed the photocurrent intensity of α-Fe_2O_3-NG without (curve a) and with (curve b) AuNRs in 0.1 M PBS (pH=7.4). Distinctly, the photocurrent intensity of α-Fe_2O_3-NG was 0.22 μA, while the photocurrent intensity of α-Fe_2O_3-NG-AuNRs increased to

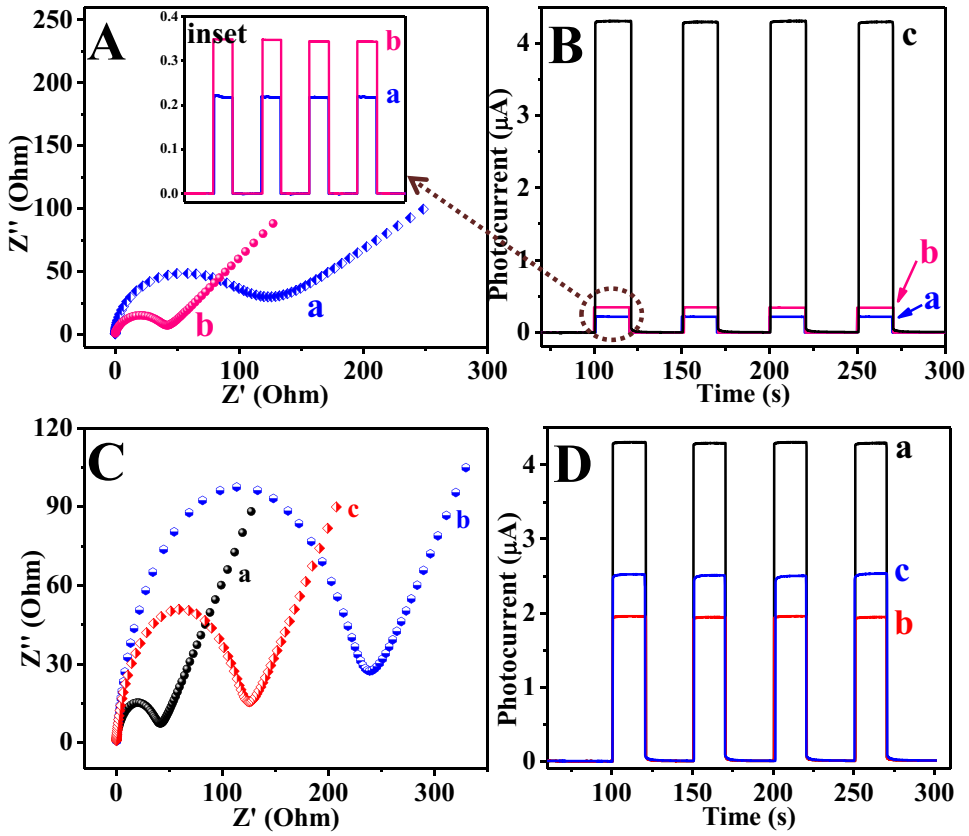

Fig. 3. (A) EIS of different modified electrode: α-Fe_2O_3-NG/ITO (a), α-Fe_2O_3-NG-AuNRs/ITO (b). (B) Photocurrent responses of α-Fe_2O_3-NG/ITO (a), α-Fe_2O_3-NG-AuNRs/ITO (b) without and (c) with 0.1 M AA in 0.1 M PBS (pH=7.4). (C) EIS of α-Fe_2O_3-NG-AuNRs/ITO (a), aptamer/α-Fe_2O_3-NG-AuNRs/ITO (b), and after the incubation with E2 (10^{-14} M) on the aptamer/α-Fe_2O_3-NG-AuNRs/ITO (c). (D) Photocurrent responses of α-Fe_2O_3-NG-AuNRs/ITO (a) and aptamer/α-Fe_2O_3-NG-AuNRs/ITO in the absence (b) and presence (c) of 10^{-14} M E2 in 0.1 M PBS (pH=7.4) containing 0.1 M AA.

0.35 μA due to the introduction of AuNRs (Fig. 3, inset). It is obvious that photocurrent intensity of α-Fe_2O_3-NG-AuNRs was almost 1.6 times higher than that of α-Fe_2O_3-NG. This was attributed to that the plasmonic AuNRs localized the incident light intensity to help increase the light absorbed by the α-Fe_2O_3-NG layer in this PEC system and thus enhance the photoactivity of α-Fe_2O_3-based electrodes (Archana et al., 2015). It was confirmed by the results of UV–vis spectrum (Fig. 1D). Particularly, owning to the SPR-induced electrical field amplification effect, the SPR-generated hot electrons were injected into the conduction band of α-Fe_2O_3 and these electrons then rapidly transferred to electrode, which in turn promoted the separation of e^-/h^+ pairs, leading to the increment of photocurrent density (Da et al., 2014). Moreover, the curve c in Fig. 3B represented the PEC responses of α-Fe_2O_3-NG-AuNRs in 0.1 M PBS (pH=7.4) supporting electrolyte solution containing 0.1 M AA. The photocurrent intensity crazily enhanced to 4.31 μA when introducing 0.1 M AA to the PBS. Herein, AA served as an electron donor for capturing photogenerated holes to enhance the photocurrent and thus maintain the photocurrent stability of the PEC aptasensor (Li et al., 2015b).

3.4. Construction of the PEC sensor for E2 detection

The properties of PEC aptasensor based on the α-Fe_2O_3-NG-AuNRs were examined upon photoexcitation with visible light. The results are shown in Fig. 3D and it can be seen that the α-Fe_2O_3-NG-AuNRs/ITO showed a strong photocurrent intensity of 4.31 μA with excellent stability (curve a), indicating that α-Fe_2O_3-NG-AuNRs hybrids were an ideal candidate material for PEC aptasensor construction. Furthermore, when aptamers assembled on the α-Fe_2O_3-NG-AuNRs/ITO surface, the photocurrent of aptamer/α-Fe_2O_3-NG-AuNRs/ITO decreased to 1.95 μA (curve b). This phenomenon can be explained as follows: with the loading of aptamer onto the α-Fe_2O_3-NG-AuNRs/ITO, photo-generated electron transfer could be blocked, thus reducing the photocurrent (curve b). When E2 was further attached on the electrode, the specific binding of target analyte E2 to aptamer caused an increase in photocurrent as shown in curve c (C_{E2}=10^{-14} M). The detection of E2 can be achieved by the constructed PEC aptasensor.

The photocurrent increased after E2 recognized by the aptamer/α-Fe_2O_3-NG-AuNRs/ITO, exhibiting a typical signal-on response. As is known to all, the conventional signal-on PEC aptasensors were realized on two primary principles either (1) target analytes induce the conformational conversion of aptamer or (2) target analytes were oxidized and thus cause the generation of high photocurrent signal (Fan et al., 2015; Li et al., 2014b). In order to explore the detection principle of the aptasensor in this work, a series of inquiry-experiments were designed. In the absence of aptamers, the photocurrent responses of the α-Fe_2O_3-NG/ITO and α-Fe_2O_3-NG-AuNRs/ITO were recorded before and after the addition of E2 to compare the PEC performances. Fig. 4A and Fig. 4B showed that after 10^{-11} M E2 added into the PEC cell, the photocurrent intensity changes of two kinds of modified electrodes were unconspicuous. Such control experiments revealed that E2 could not be oxidized by the α-Fe_2O_3-NG/ITO and α-Fe_2O_3-NG-AuNRs/ITO, eliminating the possibilities of principle (2). As a result, the detecting mechanism of aptasensor should be described as principle (1) in Scheme 1. After α-Fe_2O_3-NG-AuNRs/ITO assembling E2 aptamers, the electrode capture of E2 would lead to the conformational change of the aptamers and thus complete dissociation of some aptamers from the electrode surface, thereby decreases the electron transfer resistance between the surface of electrode and the solution and increases the photocurrent of the PEC aptasensor (Pawar et al.,

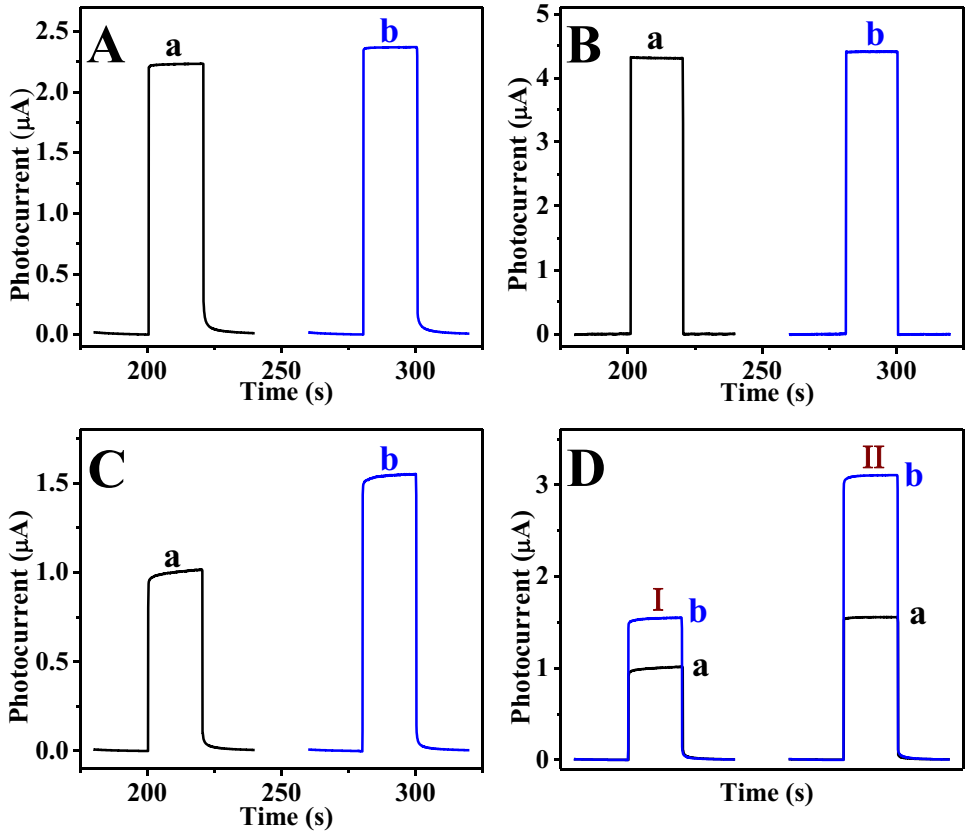

Fig. 4. Comparison of PEC responses of (A) α-Fe_2O_3-NG/ITO; (B) α-Fe_2O_3-NG-AuNRs/ITO; and (C) aptamer/α-Fe_2O_3-NG/ITO in the absence (a) and presence (b) 10^{-11} M E2 in 0.1 M PBS containing 0.1 M AA. (D) Comparison of the sensitivity of aptamer/α-Fe_2O_3-NG/ITO (I) and aptamer/α-Fe_2O_3-NG-AuNRs/ITO (II) toward 10^{-11} M E2.

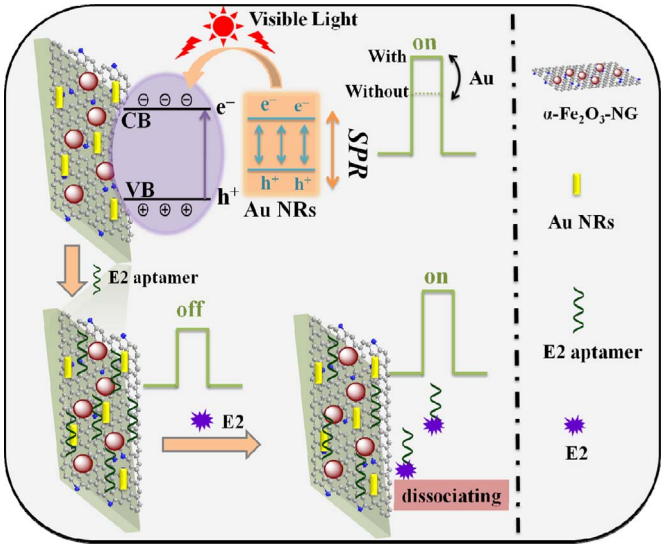

Scheme 1. Schematic representation of the fabrication of the PEC aptasensor.

2015; Fan et al., 2015), which was in good agreement with that decrement in R_{et} from EIS measurement in Fig. 3C after the aptasensor incubated with E2. Fig. 4C further confirmed the principle (1). As showed in Fig. 4C, the photocurrent intensity increased with the amount of E2 increasing on the aptamer/α-Fe_2O_3-NG/ITO surface without AuNRs, which demonstrated that upon the presence of E2, the aptamer was dissociated from the electrode surface, leading to the recovery of photocurrent signal.

Moreover, the PEC responses of aptamer/α-Fe_2O_3-NG/ITO and aptamer/α-Fe_2O_3-NG-AuNRs/ITO toward E2 were compared under the same conditions. As illustrated in Fig. 4D, the aptasensors fabricated on aptamer/α-Fe_2O_3-NG-AuNRs/ITO exhibited higher PEC response toward E2 than that immobilized on aptamer/α-Fe_2O_3-NG/ITO, demonstrating the superiority of introducing the AuNRs in fabrication of highly sensitive PEC aptasensor.

3.5. Performance of the aptasensor

In order to better evaluate the performance of the PEC aptasensor, the photocurrent change was measured in various concentrations of E2 under the optimal conditions (Suplementary material), as was shown in Fig. 5A. The photocurrent gradually increased with increasing concentrations of E2 in the range from 1×10^{-15} M to 1×10^{-9} M, indicating that more and more E2-aptamer complexes fell off and decreased the steric hindrances. In addition, the corresponding calibration curve for E2 determination was presented in Fig. 5B. The peak photocurrent (I) was linearly related with the logarithm of the concentrations of E2 with te limit of detection was 0.33 fM (S/N=3). Some detailed comparisons of the analytical performance of the E2 aptasensor for detecting E2 with other methods are given in Table S1. The sensitivity of the present method was higher than the previous reports (Moraes et al., 2015; Li et al., 2015c; Huang et al., 2015; Olowu et al., 2010; Dharuman et al., 2013; Ke et al., 2014; Fan et al., 2014).

3.6. Reproducibility, stability, and specificity of the aptasensor

The reproducibility of the aptasensor was evaluated by testing a series of five electrodes prepared in the same way. The resulting relative standard deviation (RSD) was 4.73%, indicating remarkable reproducibility of the fabrication protocol.

The stability of the aptasensor was an important factor. Time-dependent photocurrent responses of the PEC aptasensor were recorded as the excitation light was turned on and off iteratively (Fig.

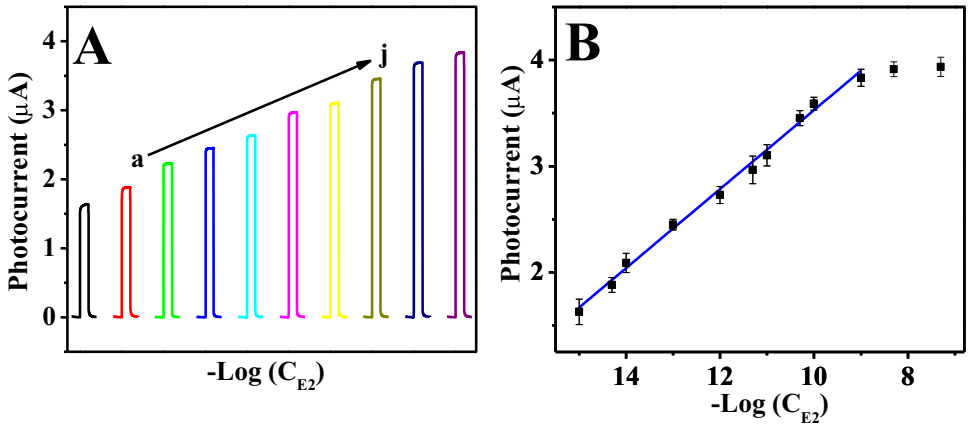

Fig. 5. (A) The relationship between the photocurrent intensity and E2 concentration. (B) The corresponding linear calibration curve for E2 detection. Error bars: ± S.D., n=5.

S6A). It was obvious that the PEC intensity was very stable over 1000 s, indicating the aptasensor can be applied in the real samples. The long-time stability of the aptasensor was also studied on a 14-day period. After kept it in refrigerator (4 °C) for 2 weeks, the aptasensor did not show an obvious change, demonstrating that the aptasensor had good stability.

The specificity of the proposed PEC aptasensor for E2 detection was also examined by detecting the photocurrent change (ΔI) of the aptasensor in presence of other interfering agents: estriol (E3), ethinylestradiol (EE), hydroquinone (HQ), and bisphenol-A (BPA). Both of E3 and EE not only have similar physical and chemical properties but very similar structures with E2. The experimental results were shown in Fig. S6B. It was found that 10^{-11} M of E2 gave significant peak current change, while 100-fold concentration of the other interfering agents had slight photocurrent change. The above results confirmed that the developed aptasensor could be used to determinate E2 with high specificity.

3.7. Practical application of aptasensor

In order to investigate the possibility of this aptasensor, milk powder samples were tested by adding different concentrations of E2 via a recovery study according to the analytical procedure in the Suplementary Material. The average amount of E2 in milk powder was 14.57 ng g^{-1} (n=3) and the details of determination results were displayed in Table S2. The recoveries were in the range of 86.96~102.94% with the RSD in the range of 2.3~7.4%. The satisfactory results demonstrated that the proposed aptasensor can be applied to the practical determination of E2 in real complex samples.

4. Conclusions

In summary, an ultrasensitive and selective PEC detection of E2 was achieved by employing ternary α-Fe_2O_3-NG-AuNRs hybrids as photoactive materials and aptamer as recognition element. The integration of AuNRs with α-Fe_2O_3-NG contributed to the high visible-light PEC activity and excellent sensitivity. After E2-binding aptamer was immobilized on α-Fe_2O_3-NG-AuNRs/ITO, an aptasensor for E2 was developed. Under the optimal conditions, the fabricated sensor exhibited high sensitivity and selectivity, low limit of detection, and long-term stability. Moreover, the aptasensor has been applied in the determination of E2 in milk powder. Such a 'signal-on' aptasensor demonstrates a novel PEC aptasensing strategy on the basis of plasmonic enhancement of PEC activity.

Acknowledgements

The present work was supported by the National Natural Science Foundation of China (Nos. 21175061, 21375050 and 21675066), a Project Funded by the Priority Academic Program Development of Jiangsu Higher Education Institutions (No. PAPD-2014-37), Qing Lan Project and Innovation Project of Science and Technology for Graduates of Jiangsu University (No. KYLX16_0907).

Appendix A. Supporting information

Supplementary data associated with this article can be found in the online version at doi:10.1016/j.bios.2017.01.034.

References

Abe, R., 2010. J. Photochem. Photobiol. C 11, 179–209.
Alsager, O.A., Kumar, S., Zhu, B., Travas-Sejdic, J., McNatty, K.P., Hodgkiss, J.M., 2015. Anal. Chem. 87, 4201–4209.
Archana, P.S., Pachauri, N., Shan, Z.C., Pan, S.L., Gupta, A., 2015. J. Phys. Chem. C 119, 15506–15516.
Citartan, M., Gopinath, S.C.B., Tominaga, J., Tan, S.C., Tang, T.H., 2012. Biosens. Bioelectron. 34, 1–11.
Da, P.M., Li, W.J., Lin, X., Wang, Y.C., Tang, J., Zheng, G.F., 2014. Anal. Chem. 86, 6633–6639.
Dai, L.M., Du, X.J., Jiang, D., Chen, W., Zhu, M.Y., Wang, K., 2017. Microchim. Acta 184, 137–145.
Deng, K.Q., Li, C.X., Li, X.F., Huang, H.W., 2016. J. Electroanal. Chem. 780, 296–302.
Dharuman, V., Hahn, J.H., Jayakumar, K., Teng, W., 2013. Electrochim. Acta 114, 590–597.
Draisci, R., Palleschi, L., Ferretti, E., Marchiafava, C., Lucentini, L., Cammarata, P., 1998. Analyst 123, 2605–2609.
Du, X.J., Jiang, D., Dai, L.M., Zhou, L., Hao, N., Qian, J., Qiu, B.J., Wang, K., 2016. Biosens. Bioelectron. 81, 242–248.
Ellington, A.D., Szostak, J.W., 1990. Nature 346, 818.
Eum, N.S., Yeom, S.H., Kwon, D.H., Kim, H.R., Kang, S.W., 2010. Sens. Actuators B 143, 784–788.
Fan, G.C., Zhu, H., Shen, Q.M., Han, L., Zhao, M., Zhang, J.R., Zhu, J.J., 2015. Chem. Commun. 51, 7023–7026.
Fan, L.F., Zhao, G.H., Shi, H.J., Liu, M.C., Wang, Y.B., Ke, H.Y., 2014. Environ. Sci. Technol. 48, 5754–5761.
Formal, F.L., Sivula, K., Grätzel, M., 2012. J. Phys. Chem. C 116, 26707–26720.
Han, Q., Shen, X., Zhu, W.Y., Zhu, C.H., Zhou, X.M., Jiang, H.J., 2016. Biosens. Bioelectron. 79, 180–186.
Ho, H.A., Leclerc, M., 2004. J. Am. Chem. Soc. 126, 1384–1387.
Huang, K.J., Liu, Y.J., Zhang, J.Z., Cao, J.T., Liu, Y.M., 2015. Biosens. Bioelectron. 67, 184–191.
Kataby, G., Cojocaru, M., Prozorov, R., Gedanken, A., 1999. Langmuir 15, 1703–1708.
Ke, H.Y., Liu, M.C., Zhuang, L., Li, Z.X., Fan, L.F., Zhao, G.H., 2014. Electrochim. Acta 137, 146–153.
Kochuveedu, S.T., Kim, D.P., Kim, D.H., 2011. J. Phys. Chem. C 116, 2500–2506.
Li, J., Tu, W.W., Li, H.B., Han, M., Lan, Y.Q., Dai, Z.H., Bao, J.C., 2014a. Anal. Chem. 86, 1306–1312.
Li, J.J., An, H.Q., Zhu, J., Zhao, J.W., 2015a. Appl. Surf. Sci. 347, 856–860.
Li, K., Lai, Y.J., Zhang, W., Jin, L.T., 2011. Talanta 84, 607–613.
Li, R.X., Liu, Y.X., Yan, T., Li, Y.Y., Cao, W., Wei, Q., Du, B., 2015b. Biosens. Bioelectron. 66, 596–602.
Li, R.Z., Liu, Y., Cheng, L., Yang, C.Z., Zhang, J.D., 2014b. Anal. Chem. 86, 9372–9375.
Li, Y., Zhao, X.R., Li, P., Huang, Y.F., Wang, J., Zhang, J.M., 2015c. Anal. Chim. Acta 884, 106–113.
Liang, H.F., Chen, W., Jiang, X.D., Xu, X., Xu, B.B., Wang, Z.C., 2014. J. Mater. Chem. A 2, 4340–4346.

Ma, Z.Y., Ruan, Y.F., Xu, F., Zhao, W.W., Xu, J.J., Chen, H.Y., 2016. Anal. Chem. 88, 3864–3871.
Mao, A.M., Kim, W.J., Kim, J.K., Shin, K., Han, G.Y., Park, J.H., 2013. Electrochim. Acta 97, 404–408.
McKeague, M., Derosa, M.C., 2012. J. Nucleic Acids 2012, 748913–748932.
Moraes, F.C., Rossi, B., Donatoni, M.C., Oliveira, K.T., Pereira, E.C., 2015. Anal. Chim. Acta 881, 37–43.
Neumann, Q., Zhang, D.M., Tam, F., Lal, S., Wittung-Stafshede, P., Halas, N.J., 2009. Anal. Chem. 81, 10002–10006.
Olowu, R.A., Arotiba, O., Mailu, S.N., Waryo, T.T., Baker, P., Iwuoha, E., 2010. Sensors 10, 9872–9890.
Pawar, R.C., Pyo, Y.J., Ahn, S.H., Lee, C.S., 2015. Appl. Catal. B 176–177, 654–666.
Pezzolato, M., Maurella, C., Varello, K., Meloni, D., Bellino, C., Borlatto, L., Corcia, D., Capra, P., Caramelli, M., Bozzetta, E., 2011. Food Control 22, 1668–1673.
Sassolas, A., Blum, L.J., Leca-Bouvier, B.D., 2011. Biosens. Bioelectron. 26, 3725–3736.
Shrestha, S.L., Casey, F.X., Hakk, H., Smith, D.J., Padmanabhan, G., 2012. Environ. Sci. Technol. 46, 11047–11053.
Song, J.C., Yang, J., Hu, X.M., 2008. J. Appl. Electrochem. 38, 833–836.
Song, K., Lee, Y., Jo, M.R., Nam, K.M., Kang, Y.M., 2012. Nanotechnology 23, 505101–505106.
Souza, F.L., Lopes, K.P., Nascente, P., Leite, E.R., 2009. Sol. Energy Mater. Sol. Cells 93, 362–368.
Tai, S.S., Welch, M.J., 2005. Anal. Chem. 77, 6359–6363.
Terne, T.A., Andersen, H., Gilberg, D., Bonerz, M., 2002. Anal. Chem. 74, 3498–3504.
Thimsen, E., Formal, F.L., Grätzel, M., Warren, S.C., 2011. Nano Lett. 11, 35–43.
Tu, W.W., Wang, W.J., Lei, J.P., Deng, S.Y., Ju, H.X., 2012. Chem. Commun. 48, 6535–6537.
Tuerk, C., Gold, L., 1990. Science 249, 505–510.
Warren, S.C., Thimsen, E., 2012. Energy Environ. Sci. 5, 5133–5146.
Yan, Z.Y., Wang, Z.H., Miao, Z., Liu, Y., 2016. Anal. Chem. 88, 922–929.
Yang, S., Wang, C., Ma, L., Peng, Y., Qu, Z., Yan, N., Chen, J., Chang, H., Li, J., 2013. Catal. Sci. Technol. 3, 161–168.
Yu, L., Zhang, Y.T., Chen, R., Zhang, D.H., Wei, X.H., Chen, F., Wang, J.X., Xu, M.T., 2015. Talanta 131, 475–479.
Zhang, H., Sun, Y., Wang, J., Zhang, J., Zhang, H.Q., Zhou, H., Song, D.Q., 2012. Biosens. Bioelectron. 34, 137–143.
Zhang, X.R., Zhao, Y.Q., Li, S.G., Zhang, S.S., 2010. Chem. Commun. 46, 9173–9175.
Zhang, Y., Shoaib, A., Li, J.J., Ji, M.W., Liu, J.J., Xu, M., Tong, B., Zhang, J.T., Wei, Q., 2016. Biosens. Bioelectron. 79, 866–873.
Zhang, Y.Y., Cao, T.C., Huang, X.F., Liu, M.C., Shi, H.J., Zhao, G.H., 2013. Electroanalysis 25, 1787–1795.
Zhao, W.W., Ma, Z.Y., Yan, D.Y., Xu, J.J., Chen, H.Y., 2012a. Anal. Chem. 84, 10518–10521.
Zhao, X.M., Zhou, S.W., Jiang, L.P., Hou, W.H., Shen, Q.M., Zhu, J.J., 2012b. Chem. Eur. J. 18, 4974–4981.
Zhou, H., Zhang, Y.Y., Liu, J., Xu, J.J., Chen, H.Y., 2012. J. Phys. Chem. C 116, 17773–17780.
Zhou, J.S., Song, H.H., Ma, L.L., Chen, X.H., 2011. RSC Adv. 1, 782–791.